SCIENTIFIC REPORTS
nature research

Check for updates

OPEN

Second magnetization peak, rhombic-to-square Bragg vortex glass transition, and intersecting magnetic hysteresis curves in overdoped $BaFe_2(As_{1-x}P_x)_2$ single crystals

L. Miu[1], A. M. Ionescu[1], D. Miu[2], M. Burdusel[1], P. Badica[1], D. Batalu[3] & A. Crisan[1]✉

The second magnetization peak (SMP) in the fourfold symmetric superconducting single crystals (such as iron pnictides and tetragonal cuprates) has been attributed to the rhombic-to-square transition (RST) of the quasi-ordered vortex solid (the Bragg vortex glass, BVG). This represents an alternative to the pinning-induced BVG disordering as the actual SMP mechanism. The analysis of the magnetic response of $BaFe_2(As_{1-x}P_x)_2$ specimens presented here shows that the SMP is not generated by the RST. However, the latter can affect the pinning-dependent SMP onset field if this is close to the (intrinsic) RST line, through the occurrence of a "shoulder" on the magnetic hysteresis curves $m(H)$, and a maximum in the temperature variation of the DC critical current density. These features disappear in AC conditions, where the vortex system is dynamically ordered in the RST domain, emphasizing the essential role of vortex dislocations for an efficient accommodation of the vortex system to the pinning landscape and the SMP development. The $m(H)$ shoulder is associated with a precipitous pinning-induced proliferation of dislocations at the RST, where the BVG elastic "squash" modulus softens. The DC magnetization relaxation indicates that the pinning-induced vortex system disordering continues above the RST domain, as the basic SMP mechanism.

Vortex pinning enhancement at high external magnetic fields H in superconducting single crystals with randomly distributed vortex pinning centres is one of the most relevant aspects for the understanding of the vortex-phase diagram of superconductors. In the case of weakly pinned specimens, one has the so called peak effect[1–6], where the maximum in the magnetic field dependence of the critical current density J_c (proportional to the irreversible magnetic moment) is rather sharp and located close to the DC irreversibility line (defined in the magnetic field-temperature T plane by a vanishing irreversible magnetization).

When vortex pinning is stronger, the peak effect is substituted by a wide second magnetization peak (SMP) in increasing H, with the onset field H_{on} and the peak field H_p far below the irreversibility line, leading to fishtail-shaped DC magnetic hysteresis $m(H)$ curves. Among many SMP mechanisms and models (see, for example,[7–20]), a pinning-induced disordering of the low-H quasi-ordered vortex solid (the Bragg vortex glass[21,22], BVG, stable against dislocation formation) has been considered to be at the origin of the SMP for various superconducting single crystals[9,14–18].

Significant progress for the understanding of the vortex phase diagram and the occurrence of the SMP has been made by considering the competition between the thermal energy, the pinning energy, and the elastic energy in the vortex system[11]. In the low-T domain, the thermal energy can be neglected, and the simple energy balance relation leads to an onset field which is independent of temperature. This is also the result of the order–disorder

[1]National Institute of Materials Physics, 077125 Magurele, Romania. [2]National Institute of Laser, Plasma, and Radiation Physics, 077125 Magurele, Romania. [3]SC Fileo Buildup SRL, 060816 Bucharest, Romania. ✉email: acrisan652@gmail.com

transition derived in Ref.[12]. It has been later shown[14] that the upward curvature of the $H_{on}(T)$ variation in the low-T range can be explained by taking into account the reduction of the effective pinning energy at low temperatures, where the probing current density is closer to J_c. This approach was suggested by the often observed time evolution of the SMP, with the characteristic fields decreasing at high relaxation levels. Since the SMP extends over a large magnetic field interval, it has been proposed that the pinning-induced BVG disordering is continuous[15,17], starting at H_{on}, where the energy for the plastic vortex deformation[23] is smaller than the effective pinning energy, and finishing at H_p, where the vortex system is amorphous. The essential point is the proliferation of dislocations in the vortex system for H between H_{on} and H_p (at large scales first), where the pinning increase is caused by the efficient accommodation of vortices to the pinning centres in the presence of vortex dislocations. This idea is strongly supported by the repeatedly reported elastic vortex creep-plastic creep crossover across the SMP[9,24–26].

Alternatively, is has been argued that in (tetragonal) $La_{2-x}Sr_xCuO_4$ single crystals, with fourfold symmetric inter-vortex interactions, the SMP is the direct result of the characteristic, structural rhombic-to-square transition (RST) of the BVG[13], in which case the upward curvature in $H_{on}(T)$ at low T results directly (see below). It is known for a long time that in certain anisotropic low-T_c superconductors (such as borocarbides, Nb, and V_3Si) the vortex solid undergoes the RST, as noted in[13]. Using small-angle neutron scattering experiments, the crossover toward a square vortex arrangement with increasing magnetic field was clearly seen in $La_{2-x}Sr_xCuO_4$[27], which may reflect the importance of the anisotropic vortex cores in the d-wave superconductors. The main aspect is the softening of the BVG elastic "squash" modulus C_{sq} at the RST line in the (H, T) plane[28], and it has been predicted in Ref.[29] that this BVG softening should lead to a maximum of the critical current density $J_c(H, T)$ in the elastic (collective) pinning regime, with

$$J_c \propto 1/C_{sq}. \tag{1}$$

However, the vortex pinning in the BVG (rhombic or square) is generally weak, and a better compliance of vortices to the pinning structure in the elastic regime may not be able to generate the observed, pronounced SMP.

The 122-type iron pnictide single crystals in H parallel to the crystallographic c axis exhibit a well-developed SMP[30,31], and the above RST-related SMP model has been extended to these fourfold symmetric superconductors, as in the case of $Ba(Fe_{0.925}Co_{0.075})_2As_2$[32] and $BaFe_2(As_{0.68}P_{0.32})_2$[33] (for which the existence of the BVG has been proven[34]). The SMP in LiFeAs (from the 111 family) received the same interpretation[35]. The anisotropic interaction with fourfold symmetry induces a rhombic rather than hexagonal vortex arrangement, which transforms into a square one when the vortex separation decreases. Thermal fluctuations assist in breaking the rhomb symmetry, lowering the transition field H_{RST} as the temperature increases. By minimizing the free energy of a square vortex lattice with respect to the elastic moduli, it was found that

$$H_{RST}(T) \propto (T_0 - T)T^{-\nu}\lambda^{2(1-\nu)}, \tag{2}$$

where λ is the London magnetic penetration depth, which is ~ 108 nm in the low-T limit for $BaFe_2(As_{0.68}P_{0.32})_2$[33], T_0 is a constant lower than the critical temperature T_c, and the exponent ν is close to unity[13]. The location of the RST line relative to H_{on} and H_p is controversial. An exclusive relationship between the SMP and the RST implies the identification of $H_{RST}(T)$ with $H_p(T)$, as proposed for $La_{2-x}Sr_xCuO_4$[13], whereas in the case of $Ba(Fe_{0.925}Co_{0.075})_2As_2$ it has been argued[32] that the RST line should lie between $H_{on}(T)$ and $H_p(T)$, where the normalized magnetization relaxation rate has a minimum.

In this context, we recall the interpretation of the SMP in the fourfold symmetric superconductors by analysing the magnetic response of $BaFe_2(As_{1-x}P_x)_2$ (P-Ba122) single crystals. It was found that the SMP cannot be generated by the (elastic) rhombic-to-square BVG transition, but the RST can influence the SMP onset field if this is close to the intrinsic RST transition field, as revealed for overdoped specimens. In such a situation, the RST manifests itself through the occurrence of a "shoulder" on the magnetic hysteresis curves $m(H)$, i.e., a relatively rapid increase of the effective pinning with increasing H for a limited magnetic field domain located just above H_{on}. The evolution of the $m(H)$ shoulder with temperature leads to the intersection of the isothermal magnetic hysteresis curves, and, consequently, to a peak in the temperature variation of the DC critical current density $J_c(T)$. The AC magnetic measurements performed by us indicate that when the vortex system is dynamically ordered in the RST domain the above features disappear. This suggests that the $m(H)$ shoulder is associated with a precipitous proliferation of dislocations in the vortex system on crossing the RST line, where the softening of the BVG elastic squash modulus appears. Analysis of the DC magnetization relaxation shows that the pinning-induced vortex-system disordering continues above the RST range, as the basic mechanism for the occurrence of the SMP in the case of superconductors with fourfold inter-vortex interactions, as well.

Results and discussion

It is well established that by increasing the P doping level beyond the optimal one (where T_c is maximum) the critical current density of P-Ba122 single crystals decreases. A quantitative analysis of the $J_c(T)$ dependence[31] indicated that the characteristic pinning mechanisms [related to the spatial variation of T_c (δT_c pinning) and the fluctuations in the charge carrier mean free path] are enhanced for optimally doped and underdoped samples. The P-Ba122 specimen thoroughly investigated here is an overdoped single crystal, with the nominal $x \sim 0.33$, denoted below P-Ba122od, which has the critical temperature $T_c = 27.5$ K (determined at the onset of the diamagnetic signal, see Methods). This is similar to the single crystal investigated in Ref.[33], for which the occurrence of the RST has been signalled using DC magnetic measurements. To highlight the specific shape of the magnetic hysteresis curves of overdoped samples, an optimally doped single crystal (P-Ba122op, $x \sim 0.30$, $T_c = 29$ K), with stronger pinning, has been considered.

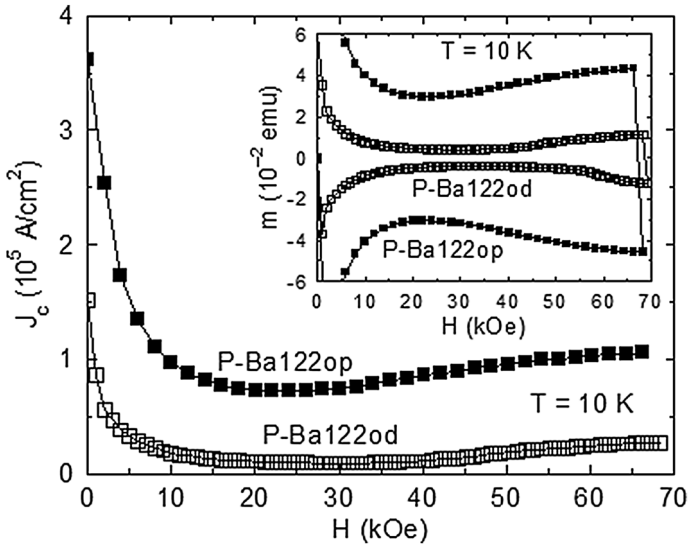

Figure 1. Main panel: Magnetic field H variation of the DC critical current density J_c determined for the optimally doped specimen P-Ba122op and the overdoped single crystal P-Ba122od (of similar dimensions) from the descending branches of the magnetic hysteresis curves $m(H)$ at the temperature $T = 10$ K plotted in the inset. The particular difference between the DC magnetic hysteresis curves $m(H)$ from the inset is that in the case of P-Ba122od there is a wide H range of weak collective (elastic) pinning in the low-field quasi-ordered vortex solid (the Bragg vortex glass), followed by a precipitous increase of $|m|$ at $H \sim 60$ kOe on the ascending $m(H)$ branch.

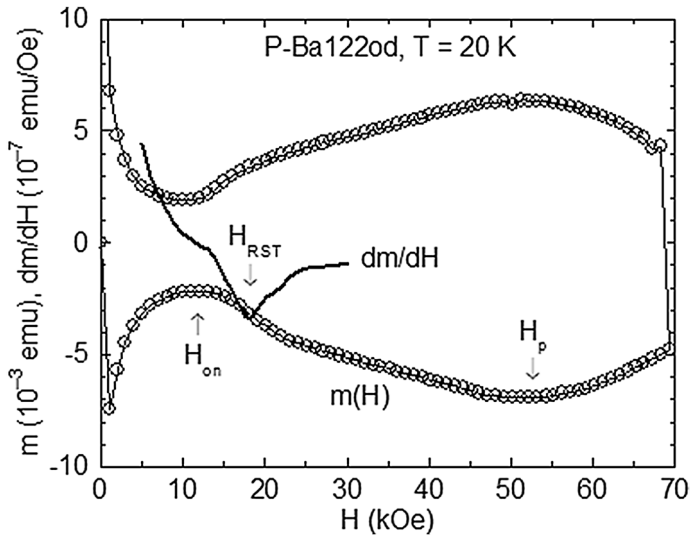

Figure 2. The DC magnetic hysteresis curve $m(H)$ of P-Ba122od at $T = 20$ K, with the onset field H_{on} and the peak field H_p of the SMP indicated by arrows. We associate the structural rhomb-to-square vortex phase transition with the "step-like" enhancement of $|m|$ in increasing H, giving rise to an $m(H)$ shoulder. The structural transition field H_{ST} has been taken at the local minimum of dm/dH (represented by a continuous line).

Figure 1 (main panel) illustrates the $J_c(H)$ variation for P-Ba122od and P-Ba122op at $T = 10$ K, where J_c has been determined with the Bean model for rectangular specimens[36] from the descending branches of the $m(H)$ curves plotted in the inset. By increasing doping from ~ 0.30 to ~ 0.33, J_c for H around the SMP onset at $T = 10$ K decreases from $\sim 7 \times 10^4$ to $\sim 10^4$ A/cm^2. The particular difference between the $m(H)$ curves of P-Ba122od and of the optimally doped specimen P-Ba122op is that in the former case there is a wide magnetic field range of weak elastic (collective) pinning (in the BVG), followed by an increase of $|m|$ around $H = 60$ kOe on the ascending $m(H)$ branch (see the inset of Fig. 1). We associate below the RST with this precipitous enhancement of the effective pinning in increasing H just above H_{on}.

The DC magnetic hysteresis curve of P-Ba122od at $T = 20$ K is plotted in Fig. 2, where H_{on} and H_p of the SMP are indicated by arrows. One notes the development of an intriguing $m(H)$ "shoulder" (leading to "pear-like"

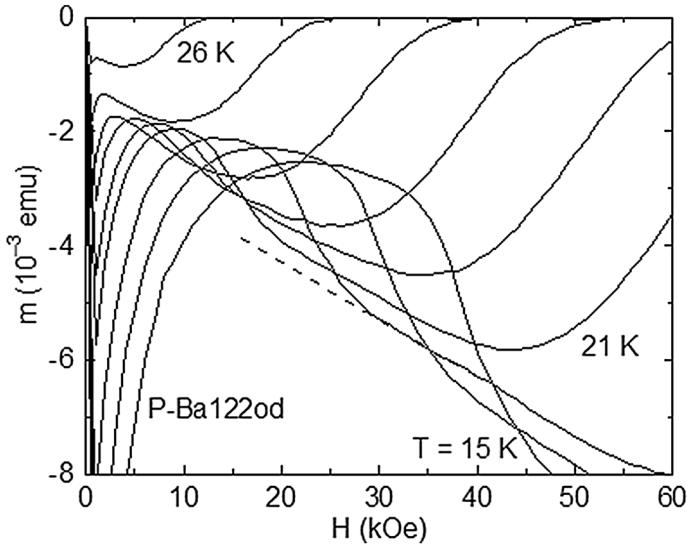

Figure 3. Evolution of the $m(H)$ shoulder in increasing H observed for P-Ba122od with decreasing temperature T (from 26 to 21 K with a step of 1 K, and from 21 to 15 K, step of 2 K), leading to the intersection of the $m(H)$ curves. The dashed line related to the $m(H)$ curve at $T = 19$ K represents a liner fit of the $m(H)$ data just above the shoulder, to estimate the width of the associated structural vortex phase transition.

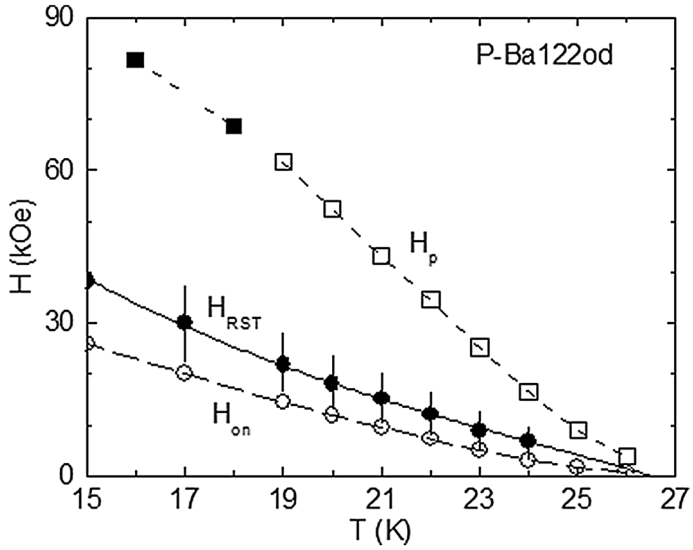

Figure 4. Temperature variation of the structural transition field H_{ST} (determined as in Fig. 2), the onset field $H_{on}(T)$, and the peak field $H_p(T)$. The vertical segments on $H_{ST}(T)$ illustrate the transition width extracted for several temperatures (by taking the structural transition symmetric relative to H_{ST}). The continuous line represents the fit of the $H_{ST}(T)$ dependence with (2), by considering the two-fluid model for the temperature variation of the magnetic penetration depth. The filed-symbol $H_p(T)$ values have been determined from the magnetic hysteresis curves registered with the PPMS.

shaped hysteresis curves), which was observed for other overdoped P-Ba122 and K-Ba122 specimens[31]. The $m(H)$ shoulder exhibits history effects. On the descending $m(H)$ branch, the vortex system seems to remain trapped in more strongly pinned high-H states (see the inset of Fig. 1). For this reason, we considered the shoulder on the ascending $m(H)$ branch, and the transition field H_{RST} has been taken at the local minimum of dm/dH, as illustrated in Fig. 2.

The evolution of the $m(H)$ shoulder with temperature is depicted in Fig. 3. As T decreases, the collective pinning in the rhombic BVG of P-Ba122od remains weak and the $m(H)$ shoulder becomes more pronounced, generating the intersection of the $m(H)$ curves (Fig. 3). The dashed line on the $m(H)$ curve at $T = 19$ K illustrates a linear fit of the $m(H)$ data just above the shoulder, to estimate the transition width. The temperature variation of the transition field H_{RST} determined as in Fig. 2, $H_{on}(T)$, and $H_p(T)$ are plotted in Fig. 4. The vertical segments on

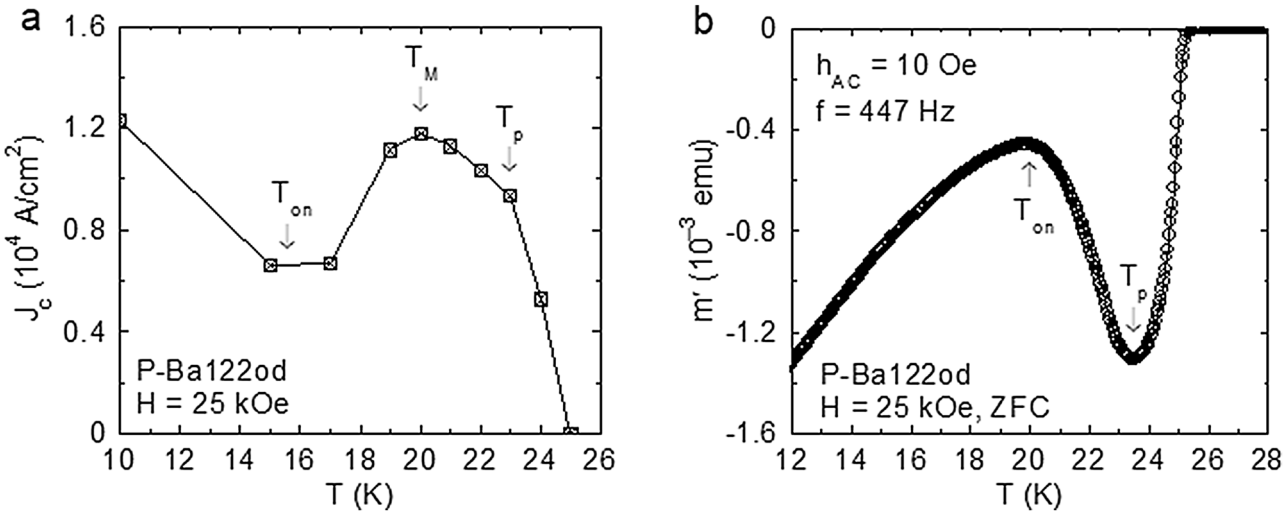

Figure 5. (**a**) Temperature variation of the DC critical current density $J_c(T)$ determined with the Bean model using the magnetic moment $m(T)$ of P-Ba122od in $H = 25$ kOe, with m taken from the isothermal magnetic hysteresis curves $m(H)$ registered at different T values (Fig. 3). The DC onset temperature T_{on} (around 16 K) and the DC peak temperature $T_p = 23$ K represent, in agreement with the $m(H)$ curves from Fig. 3, the T values where the applied field $H = 25$ kOe equals $H_{on}(T)$ and $H_p(T)$, respectively. The $J_c(T)$ maximum at $T_M = 20$ K (between T_{on} and T_p) is directly related to the $|m(T)|$ values where the $m(H)$ shoulder is completed, and, due to the large transition width, T_M is significantly higher that the structural transition temperature $T_{RST}(H = 25$ kOe) ~ 18 K in Fig. 4. (**b**) Temperature dependence of the in-phase component m' of the AC magnetic moment (directly related to the density of the macroscopic screening currents) for P-Ba122od in $H = 25$ kOe (ZFC, $h_{AC} = 10$ Oe, $f = 447$ Hz). The onset temperature T_{on} and the peak temperature T_p (indicated by arrows) correspond to the SMP generated in the sample region penetrated by the AC critical state (see text). Note that in **b** there is no feature to correspond to the $J_c(T)$ maximum at T_M in **a**.

$H_{RST}(T)$ represent the transition width extracted for several T values (by considering the RST symmetric relative to H_{RST}), showing that H_{on} is close to the lower H edge of the RST. One notes the upward curvature on $H_{RST}(T)$, which is no longer present on $H_p(T)$ below ~ 21 K. The $H_{RST}(T)$ dependence determined by us is in agreement with (2), by considering the two-fluid model for $\lambda(T)$[23,33]. The fit of the $H_{RST}(T)$ variation from Fig. 4 supplies $T_0 = 26.5$ K $< T_c$, and $\nu = 0.8$ (close to unity), as predicted by the RST theory[13]). At this point, it is worthy to note that if one takes H_{RST} as the field value where the shoulder in $|m(H)|$ is completed in increasing H, it results $T_0 > T_c$, which is in conflict with (2).

For intersecting isothermal $m(H)$ curves, the $m(T)$ variation obtained for a constant H with m taken from the magnetic hysteresis curves registered at different T values is obviously nonmonotonic, leading to a $J_c(T)$ peak, as illustrated in Fig. 5a for $H = 25$ kOe. When $m(T)$ is directly measured in increasing T at a constant H applied in ZFC conditions, the nonmonotonic dependence does not appear[33]. This is because the external magnetic field is kept constant, and no inductive processes to bring the screening current density close to the critical value J_c are present. Thus, by entering a domain of stronger pinning, one can get at most a slowdown of the magnetic relaxation, i.e., a slower decrease of $|m|$ with increasing temperature.

On the $J_c(T)$ variation from Fig. 5a one can distinguish the DC SMP onset temperature T_{on} around 16 K, and the DC peak temperature $T_p = 23$ K, representing, in agreement with the $m(H)$ curves from Fig. 3, the T values where the applied field $H = 25$ kOe equals $H_{on}(T)$ and $H_p(T)$, respectively. The $J_c(T)$ maximum at $T_M = 20$ K (located between T_{on} and T_p) is directly related to the $|m(T)|$ values where the $m(H)$ shoulder is completed, and, due to the large transition width, T_M is significantly higher that $T_{RST}(H = 25$ kOe) ~ 18 K in Fig. 4.

The main issue is to find out if the $m(H)$ shoulder [leading to the DC $J_c(T)$ maximum at T_M in Fig. 5a] corresponds, through (1), to the RST in the elastic pinning regime[29]. Alternatively, in the SMP model based on the pinning-induced BVG disordering[14,15,17,18], this can be the result of a precipitous proliferation of dislocations at the RST, where the BVG elastic squash modulus softens[28]. At this point, the use of AC magnetic measurements becomes helpful, offering the possibility to have an unambiguously ordered (dislocation free) vortex system across the RST domain. The dynamic ordering of the vortex system (i.e., healing of dislocations) at high drives[37,38] and "shaking" the vortices[39] has been proven. For this purpose, the presence of the nonlinear AC magnetic response with a large AC critical-state penetration is essential. It has been recently shown[40] that when pinning is strong and the demagnetization effects are negligible the AC magnetic signal at usual frequencies and amplitudes remains in the linear (Campbell) regime[41] up to close to the irreversibility line, and the SMP (a bulk phenomenon) does not develop, regardless of the H and T setting protocol. The situation changes drastically for P-Ba122od, due to the relatively weak pinning and pronounced demagnetization effects in perpendicular magnetic fields, where the AC field amplitude at the sample edge is strongly enhanced. In these conditions, the nonlinear regime with a large AC critical-state penetration is reached far below the irreversibility line. For AC magnetic measurements where H is constant, the effective inductive processes during the AC cycles (enhanced by demagnetization effects) keep the screening current density close to the critical value. The SMP is generated in the sample region

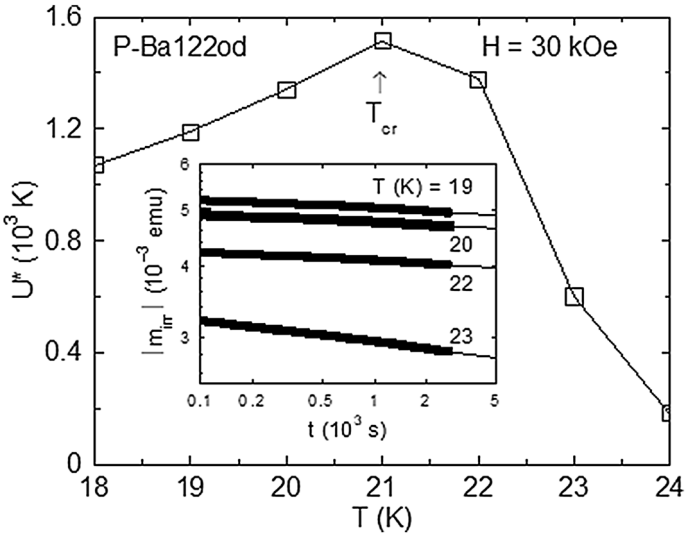

Figure 6. Inset: Time t dependence of the absolute value of the irreversible DC magnetic moment $|m_{irr}|$ in log–log scales for P-Ba122od in $H = 30$ kOe (applied in ZFC conditions) at several temperatures $T \geq 18$ K. In this representation, the relaxation curves are linear, with the slope of the linear fit (the continuous line) supplying the normalized magnetization relaxation rate $S = -d\ln(|m_{irr}|)/d\ln(t)$ and the corresponding normalized vortex-creep activation energy $U^* = T/S$. Main panel: The resulting $U^*(T)$ variation exhibits a maximum at the creep-crossover temperature T_{cr}, signalling the vortex system disordering across the second magnetization peak.

penetrated by the AC critical state, and the temperature variation of the induced current density is modulated accordingly, as presented below.

Figure 5b illustrates the temperature dependence of the in-phase component m' of the AC magnetic moment (directly related to the density J of the macroscopic screening currents[42]) for P-Ba122od in $H = 25$ kOe, obtained with the nominal AC field amplitude $h_{AC} = 10$ Oe and the frequency $f = 447$ Hz. The represented $m'(T)$ has been registered in the ZFC protocol. Actually, the FCC $m'(T)$ (not shown) and the ZFC $m'(T)$ almost overlap, indicating an extended AC critical-state penetration. The onset temperature $T_{on} \sim 20$ K (where the induced J and $|m'|$ are minimum), and the peak temperature $T_p \sim 23.5$ K (where J and $|m'|$ are maximum) in the used AC conditions correspond to the SMP generated in the sample region penetrated by the AC critical state. By difference with the DC SMP (Fig. 3), the characteristic fields for the AC SMP are shifted to higher values. In the SMP model based on the pinning-induced proliferation of dislocations, this is the manifestation of the dynamic ordering of the vortex system. The ordering effect is large at the onset of the SMP, where the dislocation density is reduced. At $H = 25$ kOe, one has the AC $T_{on} = 20$ K (Fig. 5b), which means that the AC $H_{on}(T = 20\ \text{K}) = 25$ kOe. This is considerably higher than the DC $H_{on} \sim 12.5$ kOe located on the magnetic hysteresis curve at $T = 20$ K, overcoming the upper edge of the RST (see Fig. 2). Thus, in the used AC conditions, the vortex system is ordered in the RST domain. The striking result is the absence of any significant feature on the $m'(T)$ variation which could be related to the DC $J_c(T)$ peak temperature $T_M \sim 20$ K from Fig. 5a, or, through (1), to the structural transition temperature $T_{RST}(H = 25\ \text{kOe}) \sim 18$ K (see Fig. 4). This means that the DC $J_c(T)$ peak at $T_M \sim 20$ K from Fig. 5a does not correspond to the RST in the elastic pinning regime. The effect of the elastic compliance of the BVG to the pinning landscape at the RST appears to be too small to generate the SMP. For random pinning, an efficient accommodation of vortices to the pinning centres necessitates the presence of dislocations in the vortex system. The $m(H)$ shoulder can easily be generated by a precipitous, pinning-induced vortex-system disordering triggered by the C_{sq} softening at H_{RST}, where one has a transition between the rhombic BVG and a partially dislocated (disordered) square BVG. The proliferation of dislocations at H_{RST} is favoured, since H_{RST} is close to H_{on}, where the energy balance relation should be fulfilled.

The pinning-induced vortex system disordering continues above the RST range, as indicated by the analysis of DC magnetization relaxation. The inset of Fig. 6 illustrates the relaxation time t dependence of the absolute value of the DC irreversible magnetic moment $|m_{irr}|$ in log–log scales for P-Ba122od at several temperatures in $H = 30$ kOe (applied in ZFC conditions). The considered temperature interval is above the RST domain, where the history effects are negligible. As known, when the relaxation time window t_w is moderate, in the representation from the inset of Fig. 6 the relaxation $m_{irr}(t)$ curves are linear, with the slope of the linear fit supplying the normalized magnetization relaxation rate $S = -d\ln(|m_{irr}|)/d\ln(t)$ and the corresponding normalized vortex-creep activation energy $U^* = T/S$[43,44]. For a given H well below the irreversibility line (where the pinning potential is not reduced significantly by thermal vortex fluctuations) and a fixed t_w, the $U^*(T)$ variation obtained in the framework of the general vortex creep equation is approximated by

$$U*(T) \sim U_c + pT\ln(t_w/t_0), \tag{3}$$

where U_c represents the characteristic pinning energy, p is the vortex creep exponent (positive in the case of an elastic vortex creep process[45] and negative (around $-1/2$[9]) for plastic creep, whereas t_0 is the macroscopic time scale for creep[23]. The resulting $U^*(T)$ variation, plotted in the main panel of Fig. 6, exhibits a maximum at the creep-crossover temperature T_{cr}, where, according to (3), the creep exponent changes sign, signalling the vortex system disordering across the SMP. This sign changing is possible through an increase of the characteristic pinning energy U_c, owing to a better accommodation of vortices to the pinning centres in a disordered vortex phase. The applied field $H = 30$ kOe is close to the midpoint between H_{on} and H_p at $T = T_{cr}$ (see Fig. 3), which is expected using global magnetic measurements[46].

The existence of a maximum in U^* (Fig. 6, main panel) means a minimum of the normalized magnetization relaxation $S = T/U^*$, and it is tempting to locate the RST at this S minimum[32]. However, as it can be seen in Fig. 3, there is no maximum in $|m|$ at $H = 30$ kOe on the magnetic hysteresis curve registered at $T = T_{cr} = 21$ K. Similarly, since the long-time relaxation measurements[25] and structural investigations using muon-spin rotation and small-angle neutron scattering experiments[47,48] showed that at the peak field H_p the vortex system is completely disordered, the identification of the RST line with $H_p(T)$ is ruled out.

Finally, the absence of the $m(H)$ shoulder in the case of optimally doped and underdoped single crystals (the inset of Fig. 1 and[31]) can easily be explained in terms of the pinning-induced disordering of the vortex system across the SMP. A stronger pinning will shift H_{on} well below the intrinsic $H_{RST}(T)$ line, and the RST cannot manifest in a significantly disordered vortex system.

Conclusions

In summary, we investigated the magnetic response of overdoped $BaFe_2(As_{1-x}P_x)_2$ single crystals, to clarify the relationship between the second magnetization peak and the characteristic structural rhomb-to-square transition of the Bragg vortex glass in the fourfold symmetric superconductors. It was found that the (elastic) RST does not generate the SMP, but the RST can influence the pinning-dependent SMP onset field when this is close to the intrinsic RST line, through the appearance of a shoulder on the magnetic hysteresis $m(H)$ curves. The temperature evolution of the $m(H)$ shoulder leads to the intersection of isothermal $m(H)$ curves (a rare phenomenon), and, consequently, to a peak in the temperature variation of the DC critical current density $J_c(T)$. However, this particular peak does not appear in the temperature variation of the screening current in AC magnetic measurements where the vortex system is dynamically ordered in the RST domain. This emphasizes the essential role of vortex dislocations for an effective accommodation of the vortex system to the pinning landscape and the occurrence of the SMP.

We conclude that the observed DC $m(H)$ shoulder is the effect of a precipitous pinning-induced proliferation of dislocations when the BVG elastic squash modulus softens at the structural transition between a rhombic and a partially disordered square BVG. The pinning-induced vortex-system disordering continues above the RST domain (as indicated by the magnetization relaxation results), and represents the basic SMP mechanism for the fourfold symmetric superconductors, as well. The absence of a notable effect of the RST on the SMP in the case of optimally doped and underdoped P-Ba122 single crystals can easily be explained in terms of the pinning-induced disordering of the vortex system across the SMP. The stronger pinning exhibited by optimally doped and underdoped P-Ba122 single crystals shifts the onset field well below the structural transition field, and the RST cannot manifest in a significantly disordered vortex system.

Methods

The improved quality of iron-based superconducting single crystals[49,50] made possible the observation of ordered vortex phases[34,50,51]. It is now established that the overdoped 122-type specimens exhibit a relatively weak, point-like δT_c pinning[52] and a pronounced SMP develops[31]. The P-Ba122 single crystals analysed in this work have been grown by the Ba_2As_3/Ba_2P_3-flux method[53] at the Institute of Physics, Chinese Academy of Sciences. They have been selected by the width ΔT of the diamagnetic transition in the $m'(T)$ variation registered with $H = 0$, $f = 447$ Hz, and $h_{AC} = 1$ Oe, as illustrated in Fig. 7 for P-Ba122od, where $\Delta T \sim 1$ K. The measured samples are square-shaped (with the side $l \sim 1.7$ mm), with the thickness t (in the direction of the crystallographic c axis) of ~ 50 μm.

The DC and AC magnetic fields have been oriented along the c axis, when the demagnetization factor[54] $D \sim 0.9$. Thus, the AC field amplitude h_{AC} at the sample edge is enhanced by a factor $1/(1-D) \sim 10$. The DC critical current density J_c (in A/cm^2) has been determined as $60\,|m_{irr}|/l^3t$[36], with l and t in cm, and the irreversible magnetic moment $m_{irr} = (m_+ - m_-)/2$, with m_+ (m_-) representing the magnetic moment (in emu) measured in increasing (decreasing) H. When the reversible magnetic moment is negligible, $|m_{irr}|$ can be approximated by m_-.

The DC $m(H)$ curves were usually obtained with a commercial Quantum Design Magnetic Property Measurement System (MPMS), whereas the AC magnetic moment was registered with a Physical Property Measurement System (PPMS). The presented AC results for finite H correspond to $h_{AC} = 10$ Oe, and the frequency $f = 447$ Hz. The relatively high h_{AC} and the strong demagnetization effects allow attaining the nonlinear AC regime with a large AC critical state penetration far below the DC irreversibility line of overdoped P-Ba122 single crystals.

The temperature and DC magnetic field setting followed the zero-field cooling protocol (ZFC), obtained by fast cooling the sample (~ 10 K/min) in $H = 0$ from above T_c down to $T < T_c$, then applying H, and measuring $m(H)$ or the AC magnetic signal in increasing temperature at a slow rate (~ 0.05 K/min). For comparison, the field cooling on cooling procedure (FCC) has also been used, with H applied above T_c, and then measuring the AC magnetic moment in decreasing T at the slow rate. Well below the irreversibility line, the contribution of the reversible magnetic moment to the DC $m(H)$ curves is negligible. However, in the case of magnetization

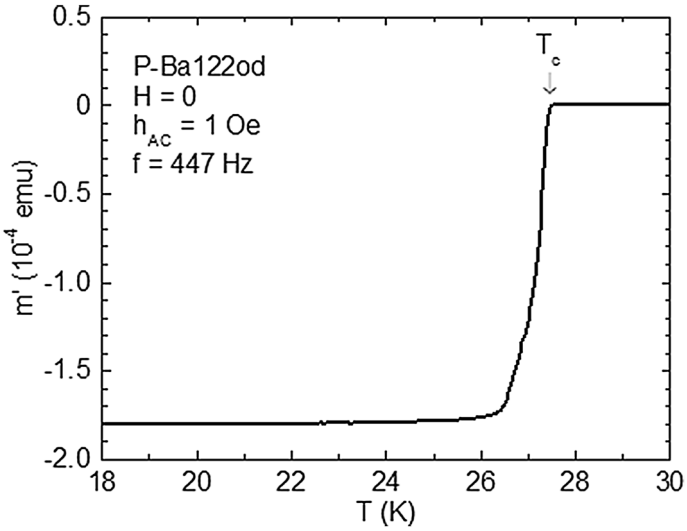

Figure 7. Temperature variation of the in-phase (screening) component m' of the AC magnetic moment for P-Ba122od in $H=0$ registered in increasing temperature with $h_{AC}=1$ Oe and $f=447$ Hz. The critical temperature T_c has be taken at the onset of the diamagnetic signal, and the width of the diamagnetic transition is around 1 K, reflecting the good quality of the thoroughly investigated single crystal.

relaxation data registered over a large temperature interval, the irreversible magnetic moment m_{irr} has been taken into account.

Data availability

The data sets that support the findings in this study are available from the corresponding author upon reasonable request.

Received: 3 June 2020; Accepted: 28 September 2020
Published online: 14 October 2020

References

1. De Sorbo, W. The peak effect in substitutional and interstitial solid solutions of high field superconductors. *Rev. Mod. Phys.* **36**, 90 (1964).
2. Pippard, A. B. A possible mechanism for the peak effect in type II superconductors. *Philos. Mag.* **19**, 217 (1969).
3. Larkin, A. I. & Ovchinnikov, Yu. N. Pinning in type II superconductors. *J. Low Temp. Phys.* **93**, 409 (1979).
4. Bermùdez, M. M. *et al.* Metastability and hysteretic vortex pinning near the order-disorder transition in $NbSe_2$: interplay between plastic and elastic energy barriers. *Phys. Rev. B* **95**, 104505 (2017).
5. Toft-Petersen, R., Abrahamsen, A. B., Balog, S., Porcar, L. & Laver, M. Decomposing the Bragg glass and the peak effect in a Type-II superconductor. *Nat. Commun.* **9**, 901 (2018).
6. Terashima, T. *et al.* Anomalous peak effect in iron-based superconductors $Ba_{1-x}K_xFe_2As_2$ ($x \approx 0.69$ and 0.76) for magnetic-field directions close to the *ab* plane and its possible relation to the spin paramagnetic effect. *Phys. Rev. B* **99**, 094508 (2019).
7. Däumling, M., Seuntjens, J. M. & Larbalestier, D. C. Oxygen-defect flux pinning, anomalous magnetization and intra-grain granularity in $YBa_2Cu_30_{7-\delta}$. *Nature* **346**, 332 (1990).
8. Krusin-Elbaum, L., Civale, L., Vinokur, V. M. & Holtzberg, F. "'Phase diagram'" of the vortex-solid phase in Y–Ba–Cu–O crystals: a crossover from single-vortex (1D) to collective (3D) pinning regimes. *Phys. Rev. Lett.* **69**, 2280 (1992).
9. Abulafia, Y. *et al.* Plastic vortex creep in $YBa_2Cu_3O_{7-x}$ crystals. *Phys. Rev. Lett.* **77**, 1596 (1996).
10. Jisra, M., Pust, L., Dlouhý, D. & Koblischka, M. R. Fishtail shape in the magnetic hysteresis loop for superconductors: interplay between different pinning mechanisms. *Phys. Rev. B* **55**, 3276 (1997).
11. Giller, D. *et al.* Disorder-induced transition to entangled vortex solid in Nd–Ce–Cu–O crystal. *Phys. Rev. Lett.* **79**, 2542 (1997).
12. Mikitik, G. P. & Brandt, E. H. Peak effect, vortex-lattice melting line, and order-disorder transition in conventional and high-T_c superconductors. *Phys. Rev. B* **64**, 184514 (2001).
13. Rosenstein, B. *et al.* Peak effect and square-to-rhombic vortex lattice transition in $La_{2-x}Sr_xCuO_4$. *Phys. Rev. B* **72**, 144512 (2005).
14. Miu, L., Adachi, T., Omori, K., Koike, Y. & Miu, D. Temperature dependence of the second magnetization peak in underdoped $La_{2-x}Sr_xCuO_4$ single crystals. *Phys. Rev. B* **82**, 064520 (2010).
15. Miu, D., Noji, T., Adachi, T., Koike, Y. & Miu, L. On the nature of the second magnetization peak in $FeSe_{1-x}Te_x$ single crystals. *Supercond. Sci. Technol.* **25**, 115009 (2012).
16. Hecher, J., Zehetmayer, M. & Weber, H. W. How the macroscopic current correlates with the microscopic flux-line distribution in a type-II superconductor: an experimental study. *Supercond. Sci. Technol.* **27**, 075004 (2014).
17. Zehetmayer, M. How the vortex lattice of a superconductor becomes disordered: a study by scanning tunnelling spectroscopy. *Sci. Rep.* **5**, 9244 (2015).
18. Zhou, W., Xing, X., Wu, W., Zhao, H. & Shi, Z. Second magnetization peak effect, vortex dynamics and flux pinning in 112-type superconductor $Ca_{0.8}La_{0.2}Fe_{1-x}Co_xAs_2$. *Sci. Rep.* **6**, 22278 (2016).
19. Galluzzi, A. *et al.* Evidence of pinning crossover and the role of twin boundaries in the peak effect in FeSeTe iron based superconductor. *Supercond. Sci. Technol.* **31**, 015014 (2018).
20. Piriou, A., Fasano, Y., Giannini, E. & Fischer, Ø. Effect of oxygen-doping on $Bi_2Sr_2Ca_2Cu_3O_{10+\delta}$ vortex matter: crossover from electromagnetic to Josephson interlayer coupling. *Phys. Rev. B* **77**, 184508 (2008).

21. Giamarchi, T. & Le Doussal, P. Phase diagrams of flux lattices with disorder. *Phys. Rev. B* **55**, 6577 (1997).
22. Sánchez, J. A. *et al.* Unveiling the vortex glass phase in the surface and volume of a type-II superconductor. *Commun. Phys.* **2**, 143 (2019).
23. Blatter, G., Fegel'man, M. V., Geshkenbein, V. B., Larkin, A. I. & Vinokur, V. M. Vortices in high-temperature superconductors. *Rev. Mod. Phys.* **66**, 1125 (1994).
24. Küpfer, H. *et al.* Peak effect and its evolution from oxygen deficiency in $YBa_2Cu_3O_{7-\delta}$ single crystals. *Phys. Rev. B* **58**, 2886 (1998).
25. Miu, L. *et al.* Crossover from elastic to plastic vortex creep across the second magnetization peak of high-temperature superconductors. *Phys. Rev. B* **62**, 15172 (2000).
26. Prozorov, R. *et al.* Vortex phase diagram of $Ba(Fe_{0.93}Co_{0.07})_2As_2$ single crystals. *Phys. Rev. B* **78**, 224506 (2008).
27. Gilardi, R. *et al.* Direct evidence for an intrinsic square vortex lattice in the overdoped high superconductor $La_{1.83}Sr_{0.17}CuO_{4+\delta}$. *Phys. Rev. Lett.* **88**, 217003 (2002).
28. Miranović, P. & Kogan, V. G. Elastic moduli of vortex lattices within nonlocal London model. *Phys. Rev. Lett.* **87**, 137002 (2001).
29. Rosenstein, B. & Knigavko, A. Anisotropic peak effect due to structural phase transition in the vortex lattice. *Phys. Rev. Lett.* **83**, 844 (1999).
30. Yang, H., Luo, H., Wang, Z. & Wen, H.-H. Fishtail effect and the vortex phase diagram of single crystal $Ba_{0.6}K_{0.4}Fe_2As_2$. *Appl. Phys. Lett.* **93**, 142506 (2008).
31. Ishida, S. *et al.* Doping-dependent critical current properties in K Co, and P-doped BaFe2As2 single crystals. *Phys. Rev. B* **95**, 014517 (2017).
32. Kopeliansky, R. *et al.* Possibility of vortex lattice structural phase transition in the superconducting pnictide $Ba(Fe_{0.925}Co_{0.075})_2As_2$. *Phys. Rev. B* **81**, 092504 (2010).
33. Salem-Sugui, S. Jr. *et al.* Observation of an anomalous peak in isofield $M(T)$ curves in $BaFe_2(As_{0.68}P_{0.32})_2$ suggesting a phase transition in the irreversible regime. *Supercond. Sci. Technol.* **28**, 055017 (2015).
34. Morisaki-Ishii, R. *et al.* Vortex lattice structure in $BaFe_2(As_{0.67}P_{0.33})2$ via small-angle neutron scattering. *Phys. Rev. B* **90**, 125116 (2014).
35. Pramanik, A. K. *et al.* Fishtail effect and vortex dynamics in LiFeAs single crystals. *Phys. Rev. B* **83**, 094502 (2011).
36. Gyorgy, E. M., van Dover, R. B., Jackson, K. A., Schneemeyer, L. F. & Waszczak, J. V. Anisotropic critical currents in $Ba_2YCu_3O_7$ analyzed using an extended Bean model. *Appl. Phys. Lett.* **55**, 283 (1989).
37. Bhattacharya, S. & Higgins, M. J. Dynamics of a disordered flux line lattice. *Phys. Rev. Lett.* **70**, 2617 (1993).
38. Miu, L. Ordering of the creeping vortex system in $Bi_2Sr_2CaCu_2O_{8+\delta}$ single crystals at low temperatures. *Phys. Rev. B* **72**, 132502 (2005).
39. Valenzuela, S. O., Maiorov, B., Osquiguil, E. & Bekeris, V. Elastic-to-plastic crossover below the peak effect in the vortex solid of $YBa_2Cu_3O_7$ single crystals. *Phys. Rev. B* **65**, 060504(R) (2002).
40. Miu, L. *et al.* AC magnetic response of superconducting single crystals exhibiting a second peak on the DC magnetization curves. *Physica C* **555**, 1 (2018).
41. Campbell, A. M. The response of pinned flux vortices to low frequency fields. *J. Phys. C* **2**, 149 (1969).
42. Clem, J. R. & Sanchez, A. Hysteretic ac losses and susceptibility of thin superconducting disks. *Phys. Rev. B* **50**, 9355 (1994).
43. Yeshurun, Y., Malozemoff, A. P. & Shaulov, A. Magnetic relaxation in high-temperature superconductors. *Rev. Mod. Phys.* **68**, 911 (1996).
44. Wen, H.-H. *et al.* Field induced vanishing of the vortex glass temperature in $Tl_2Ba_2CaCu_2O_8$ thin films. *Phys. Rev. Lett.* **79**, 1559 (1997).
45. Feigel'man, M. V., Geshkenbein, V. B., Larkin, A. I. & Vinokur, V. M. Theory of collective flux creep. *Phys. Rev. Lett.* **63**, 2303 (1989).
46. Ionescu, A. M., Miu, D., Crisan, A. & Miu, L. Pinning-induced vortex-system disordering at the origin of the second magnetization peak in superconducting single crystals. *J. Supercond. Novel Magn.* **31**, 2329 (2018).
47. Divakar, U. *et al.* Direct observation of the flux-line vortex glass phase in a type II superconductor. *Phys. Rev. Lett.* **92**, 237004 (2004).
48. Demirdiş, S., van der Beek, C. J., Mühlbauer, S., Su, Y. & Wolf, T. SANS study of vortex lattice structural transition in optimally doped $(Ba_{1-x}K_x)Fe_2As_2$. *J. Phys. Condens. Matter* **28**, 425701 (2016).
49. Fang, L. *et al.* Doping- and irradiation-controlled pinning of vortices in $BaFe_2(As_{1-x}P_x)_2$ single crystals. *Phys. Rev. B* **84**, 140504(R) (2011).
50. Demirdiş, S. *et al.* Disorder, critical currents, and vortex pinning energies in isovalently substituted $BaFe_2(As_{1-x}P_x)_2$. *Phys. Rev. B* **87**, 094506 (2013).
51. Park, A. *et al.* Effects of 6 MeV proton irradiation on the vortex ensemble in $BaFe_2(As_{0.67}P_{0.33})_2$ revealed through magnetization measurements and real-space vortex imaging. *Phys. Rev. B* **101**, 224507 (2020).
52. Liu, Y. *et al.* Doping evolution of the second magnetization peak and magnetic relaxation in $(Ba_{1-x}K_x)Fe_2As_2$. *Phys. Rev. B* **97**, 054511 (2018).
53. Nakajima, M. *et al.* Growth of $BaFe_2(As_{1-x}P_x)_2$ single crystals ($0 \le x \le 1$) by Ba_2As_3/Ba_2P_3-flux method. *J. Phys. Soc. Jpn.* **81**, 104710 (2012).
54. Brandt, E. H. Thin superconductors in a perpendicular magnetic ac field: general formulation and strip geometry. *Phys. Rev. B* **49**, 9024 (1994).

Acknowledgements

Work supported by the European Regional Development Fund, Operational Program Competitiveness, POC Project P_37_697 (28/01.09.2016), and by the Romanian Ministry of Research and Innovation through the projects 12PFE/2018 and PN19-030101. We are grateful to D. Hu, S.-L. Li and H.-Q. Luo from the Institute of Physics, Chinese Academy of Sciences, for providing us with the P-Ba122 single crystals, and to J. Mosqueira from University of Santiago de Compostela, Spain, for help with some of the PPMS measurements. LM acknowledges the kind assistance of the Alexander von Humboldt Foundation.

Author contributions

A.M.I., D.M., M.B., D.B., and P.B. performed the DC magnetic measurements and carried out the analysis of magnetization relaxation. A.C. measured the AC magnetic response, and L.M. wrote the paper with contributions of all authors.

Competing interests

The authors declare no competing interests.

Additional information

Correspondence and requests for materials should be addressed to A.C.

Reprints and permissions information is available at www.nature.com/reprints.

Publisher's note Springer Nature remains neutral with regard to jurisdictional claims in published maps and institutional affiliations.

Open Access This article is licensed under a Creative Commons Attribution 4.0 International License, which permits use, sharing, adaptation, distribution and reproduction in any medium or format, as long as you give appropriate credit to the original author(s) and the source, provide a link to the Creative Commons licence, and indicate if changes were made. The images or other third party material in this article are included in the article's Creative Commons licence, unless indicated otherwise in a credit line to the material. If material is not included in the article's Creative Commons licence and your intended use is not permitted by statutory regulation or exceeds the permitted use, you will need to obtain permission directly from the copyright holder. To view a copy of this licence, visit http://creativecommons.org/licenses/by/4.0/.

© The Author(s) 2020